AIAA JOURNAL
Vol. 47, No. 6, June 2009

Reduction of Wind Turbine Noise Using Optimized Airfoils and Trailing-Edge Serrations

Stefan Oerlemans*
National Aerospace Laboratory/NLR, 8300 AD Emmeloord, The Netherlands
Murray Fisher†
GE Energy, Greenville, South Carolina 29615
Thierry Maeder‡
GE Global Research, 85748 Munich, Germany
and
Klaus Kögler§
GE Energy, 48499 Salzbergen, Germany

DOI: 10.2514/1.38888

Acoustic field measurements were carried out on a 94-m-diam three-bladed wind turbine with one standard blade, one blade with trailing-edge serrations, and one blade with an optimized airfoil shape. A large horizontal microphone array, positioned at a distance of about one rotor diameter from the turbine, was used to locate and quantify the noise sources in the rotor plane and on the individual blades. The acoustic source maps show that for an observer at the array position, the dominant source for the baseline blade is trailing-edge noise from the blade outboard region. Because of convective amplification and directivity, practically all of this noise is produced during the downward movement of the blade, which causes the typical swishing noise during the passage of the blades. Both modified blades show a significant trailing-edge noise reduction at low frequencies, which is more prominent for the serrated blade. However, the modified blades also show tip noise at high frequencies, which is mainly radiated during the upward part of the revolution and is most important at low wind speeds due to high tip loading. Nevertheless, average overall noise reductions of 0.5 and 3.2 dB are obtained for the optimized blade and the serrated blade, respectively.

Nomenclature

D	=	trailing-edge noise directivity function
f	=	frequency
M	=	local blade inflow Mach number
N	=	number of measurements
P	=	rotor power
St	=	Strouhal number ($f \cdot \delta^* / U$)
U	=	local blade inflow velocity
$U10$	=	wind speed at 10 m height
α	=	misalignment angle between array and wind turbine
δ^*	=	trailing-edge boundary-layer displacement thickness
ε	=	standard deviation of the mean (standard error) ($\sigma/\sqrt{N}$)
θ	=	angle between blade chord line and source-observer line
ξ	=	angle between blade flow velocity and source-observer line
σ	=	standard deviation
φ	=	angle between blade plane and plane containing chord line and observer
ψ	=	blade azimuth angle

Presented as Paper 2819 at the 14th AIAA/CEAS Aeroacoustics Conference, Vancouver, Canada, 5–7 May 2008; received 2 June 2008; revision received 23 February 2009; accepted for publication 24 February 2009.

*Research Engineer, Aeroacoustics Group, P.O. Box 153.
†Research Engineer, Advanced Aero & Acoustics Technologies, 300 Garlington Road.
‡Research Engineer, Alternative Energy and Environmental Technologies, Freisinger Landstrasse 50.
§Research Engineer, Advanced Aero & Acoustics Technologies, Holsterfeld 16.

I. Introduction

WIND turbine noise is one of the major issues for the widespread use of wind energy. For a modern large wind turbine, aerodynamic noise from the blades is generally considered to be the dominant noise source, provided that mechanical noise is adequately treated [1]. The sources of aerodynamic noise can be divided into airfoil self-noise and inflow-turbulence noise. Airfoil self-noise is the noise produced by the blade in an undisturbed inflow and is caused by the interaction between the boundary layer and the trailing edge of the blade. Self-noise can be tonal or broadband in character and may be caused by several mechanisms, such as turbulent boundary-layer/trailing-edge interaction noise (subsequently denoted as trailing-edge noise), laminar boundary-layer vortex-shedding noise, trailing-edge bluntness noise, or blade tip noise. Inflow-turbulence noise is caused by the interaction of upstream atmospheric turbulence with the blade and depends on the atmospheric conditions. It is an open issue to what extent inflow-turbulence noise contributes to the overall sound level of a wind turbine [2].

Because of the large number of applications (e.g., wind turbines, airplanes, helicopters, and fans), the characteristics of airfoil noise have been investigated extensively in both experimental and theoretical studies [3–13]. Both inflow-turbulence and self-noise mechanisms were considered and the dependence on parameters such as flow speed, angle of attack, radiation direction, and airfoil shape was characterized. These studies formed the basis of several semi-empirical wind turbine noise prediction models, which were validated by comparison with field measurements [14–20]. Because the field results only provided the overall sound level of the turbine, the relative importance of the different mechanisms was determined mainly on the basis of the predictions. In some studies, inflow-turbulence noise was regarded to be the dominant source [11,14–16,18], whereas others considered trailing-edge noise to be dominant [17]. In another case, the turbine noise in different frequency ranges was attributed to mechanical noise, trailing-edge noise, tip noise, and inflow-turbulence noise [19].

In a few studies, source location measurements were performed to provide more direct information on the source mechanisms [21–25]. The results from [21–23] were obtained using an acoustic parabola or a linear array of microphones and focused only on the horizontal (downward) blade position ($\psi = 90$ deg). In [24,25], a large two-dimensional microphone array, positioned on the ground about one rotor diameter upwind of the turbine, was used to localize the noise sources in the complete rotor plane and on the individual blades for two different wind turbines. It was shown that practically all recorded noise was produced during the downward movement of the blades. This strongly asymmetric source pattern, which causes the typical swishing noise during the passage of the blades, was explained by convective amplification and trailing-edge noise directivity. The following directivity function for trailing-edge noise was used [26]:

$$D = \frac{2\sin^2(\theta/2)\sin^2\varphi}{(1 - M\cos\xi)^4} \tag{1}$$

where θ is the angle between the blade chord line and the source-observer line, φ is the angle between the plane of the blade and the plane containing the chord line and the observer, ξ is the angle between the (inverted) local blade inflow velocity and the source-observer line, and M is the local blade inflow Mach number (see Fig. 1 for definition of angles). The numerator in Eq. (1) describes the directivity of high-frequency trailing-edge noise and indicates that most of the noise is radiated in the direction of the airfoil leading edge. It was analytically derived for edge noise from a semi-infinite flat plate [6,27], but was also found to be valid for finite airfoils [9], provided that the angle θ is not too close to 180 deg. In the limit for low-frequency dipole noise, for which the acoustic wavelength is much larger than the airfoil chord, the $\sin^2(\theta/2)$ term changes into $\sin^2(\theta)$ [5,26]. Nevertheless, in [24], Eq. (1) was found to be valid for the whole tested frequency range, including the low frequencies, for which the acoustic wavelength was of the same order as the blade chord. The denominator in Eq. (1) represents the fourth-power convective amplification factor for trailing-edge noise [28] and indicates that the noise source becomes louder when it is moving toward the observer.

Many studies have addressed the reduction of airfoil or wind turbine noise. Because inflow-turbulence noise and trailing-edge noise both scale with approximately the fifth power of the local blade inflow velocity [5,6,24], an obvious means for noise reduction is to reduce the rotor rpm or rotor diameter. However, these measures also reduce the power output of the turbine [1]. The same holds for increasing the blade pitch angle (i.e., turning the blade leading edge against the wind): this reduces the local angle of attack and therefore the noise, but (due to the reduced lift) also the power production. Thus, the challenge is to achieve a noise reduction without a reduction in power output. With regard to tip noise, which depends on the characteristics of the tip vortex, it has been demonstrated in several studies that the tip shape can have a significant influence on the noise from a wind turbine [1,6]. The importance of inflow-turbulence noise depends on the structure of the atmospheric turbulence and on the shape of the blades. It has been shown both experimentally and numerically that inflow-turbulence noise levels increase with increasing sharpness of the airfoil leading edge [10,13].

With regard to trailing-edge noise, a number of reduction concepts have been investigated. After it had been shown theoretically that the acoustic radiation efficiency of a trailing edge can be reduced by serrations [29] (see Fig. 2), this concept was investigated in a number of experimental studies on 2-D airfoils [30], model wind turbines [31,32], and a full-scale wind turbine [23]. In [31], serrations were applied to a 16-m-diam model wind turbine and, depending on the flow conditions, overall noise reductions of up to 3.5 dB were obtained. To prevent increased noise at high frequencies, it was found to be critical to align the plane of the serrations with the trailing-edge flow. In [23], serrations were applied to a 1 MW wind turbine, and an overall noise reduction of 2–3 dB was obtained, despite increased noise at high frequencies. It should be noted that the measurements in [23,31] only focused on the horizontal (downward) blade position ($\psi = 90$ deg), which may give an incomplete picture.

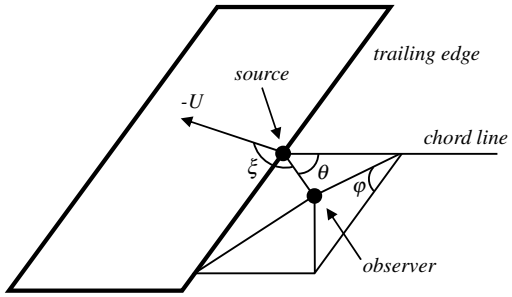

Fig. 1 Definition of angles for trailing-edge noise source.

Fig. 2 Climber removing trips from serrated blade.

An alternative concept for trailing-edge noise reduction is the application of flexible trailing-edge brushes. The brushes align automatically with the trailing-edge flow and have shown significant noise-reduction potential in wind-tunnel tests on flat plates and on a 2-D airfoil [12,33]. However, a first attempt to apply this concept to a full-scale wind turbine yielded a reduction of only 0.5 dB [34], possibly because the improvised brushes were too short. Finally, it has been shown in calculations and wind-tunnel tests on 2-D airfoils that trailing-edge noise can be reduced by a modification of the airfoil shape, without a loss in aerodynamic performance [35]. Note that in the case of an acoustically optimized airfoil shape, trailing-edge noise is reduced by changing the structure of the boundary-layer turbulence, whereas serrations or brushes are meant to affect only the scattering at the trailing edge. Thus, the effects of an optimized airfoil shape and brushes or serrations are expected to supplement each other.

The present study concerns acoustic field measurements on a 2.3 MW, 94-m-diam wind turbine with one standard (baseline) blade, one blade with an acoustically optimized airfoil shape, and one standard blade with trailing-edge serrations. The tests were performed in the framework of the European SIROCCO (Silent Rotors by Acoustic Optimisation) project [34]. Building on the results from earlier wind-tunnel studies on a model rotor [32], the subject of the project was the design, testing, and full-scale validation of quiet wind turbine blades, without a loss in power performance. In an earlier stage of the project, acoustic field measurements on the baseline turbine [25] indicated that trailing-edge noise from the outer 25% of the blades was the dominant noise source for this turbine and that the three blades produced practically the same sound pressure levels: the average overall sound pressure level (OASPL) for the three blades differed by less than 0.15 dB and, for the two standard blades that were used again in the present campaign, less than 0.05 dB.

Subsequently, optimized airfoil shapes were designed and assessed through aerodynamic and acoustic wind-tunnel tests on 2-D airfoils [34–36]. The principle of the airfoil design was to reduce the dominant low-frequency (less than 1 kHz) trailing-edge noise peak in the spectrum (which is due to the thick suction-side boundary layer) by reducing the loading of the suction side, at the expense of an increased pressure-side loading (which causes a slightly higher noise level at less important medium frequencies of 1–3 kHz) [35]. The wind-tunnel tests showed 2–3 dB reduction in OASPL (depending on lift coefficient) [34] and an improved aerodynamic performance for the newly designed airfoils, even though severe geometric and aerodynamic constraints had to be considered in the design (to enable implementation in the existing blade structure). The new airfoil was then incorporated in the design of the outer part of the optimized blade (subsequently denoted as the SIROCCO blade). The twist distribution of the SIROCCO blade was modified such that the lift distribution was approximately the same as for the baseline blade. In addition to the new blade design, the third rotor blade was used to test a second noise-reduction concept, trailing-edge serrations. The serrated blade had the same nominal geometry as the baseline blade (including the twist distribution). From power and loads measurements on the baseline and modified rotors, it was found that the in-plane and out-of-plane blade loads on the serrated blade (and, to a lesser extent, also on the SIROCCO blade) were slightly higher than on the baseline blade, causing the aerodynamic performance of the modified blades to be similar or slightly better than the baseline blade [34].

The main goal of the present test campaign was to assess the acoustic performance of the two modified blades versus the baseline blade. To assess the effect of blade roughness due to dirt or insects, the blades were tested in both clean and tripped conditions. A large horizontal microphone array, positioned at a distance of about one rotor diameter from the turbine, was used to measure the distribution of the noise sources in the rotor plane and on the individual blades. Because the array position was fixed and the wind direction varied, both up- and downwind measurements were performed. In the present paper, the acoustic array results are presented and analyzed. The noise characteristics for the three blades are investigated as a function of wind speed, rotor azimuth angle, and observer position (upwind or downwind), for clean and tripped conditions. Section II describes the test setup, test program, and the array processing methods. In Sec. III, the results are presented and discussed. The conclusions of this study are summarized in Sec. IV.

II. Experimental Method

A. Test Setup

The measurements were carried out in March/April 2007 on the same General Electric 2.3 MW prototype test wind turbine that was used in the baseline test campaign in 2005. It had a rotor diameter of 94 m, a tower height of 100 m, and was located on the Netherlands Energy Research Foundation test site in the Wieringermeer (The Netherlands). The turbine control system adjusted the rpm and blade pitch angle, depending on the wind speed measured at the nacelle: for higher wind speeds, the pitch angle was increased, reducing the local angle of attack and thus the blade loading. The rpm increased up to a certain wind speed, after which it remained constant. The turbine had a yaw mechanism that automatically turned the rotor against the wind.

To compare the blade performance for identical weather and turbine conditions, the rotor consisted of one standard (baseline) blade, one standard blade with trailing-edge serrations, and one SIROCCO blade. The SIROCCO blade was nominally identical to the baseline blade, except for the outer $\sim$30%, where it had a new airfoil. The serrated blade had the same nominal geometry as the baseline blade. The aluminum serrations, with a thickness of 2 mm, were mounted to the outer 12.5 m of the blade on the pressure side. The 2 mm step was smoothed using filler material over a few centimeters of chord. Similar to [32], the length of the serrations was about 20% of the local chord and varied as a function of radius: the tooth length was about 10 cm at the tip and about 30 cm at the most inboard position. A picture of the serrated blade is shown in Fig. 2. Using templates for different radial stations, the plane of the serrations was aligned with the flow direction at the blade trailing edge (as determined from flow calculations). This trailing-edge flow direction is constant in the variable-rpm region of the turbine. By aligning the serrations with the flow, it was attempted to minimize their aerodynamic impact and prevent increased high-frequency noise by flow through the teeth. Before the acoustic measurements, all blades were cleaned. To assess the effect of blade roughness due to dirt or insects, the blades were tested with and without trips: in state 1 all blades were tripped and in state 2 all blades were clean. The 2-D trips, with a thickness of about 0.4 mm and a width of 4 mm, were installed close to the leading edge on both sides of the blade, from the very tip to about half the blade span. The (variable) blade pitch angle was the same for the three blades.

An acoustic array was used to locate and quantify the noise sources on the rotor and on the individual blades. The acoustic array consisted of 148 Panasonic WM-61 microphones, mounted on a horizontal wooden platform of 16×18 m^2, which was positioned at a distance of about one rotor diameter from the turbine (Fig. 3). Because the array position was fixed and the wind direction varied, both up- and downwind measurements were performed. The Panasonic microphones were mounted flush to the surface of the platform, with the membrane parallel to the platform, and were equipped with wind screens. As a reference, two calibrated LinearX M51 microphones equipped with hemisphere wind screens were mounted on the platform as well. To correct for the view angle of about 45 deg (Fig. 3), the microphone array had an elliptic shape (Fig. 4), rather than the conventional round array design. In this way, the effective array shape, as seen from the rotor, is round, so that the resolution with which the noise sources in the rotor plane are localized is approximately the same in the horizontal and vertical directions. The ellipse was slightly tilted to the right-hand side of the rotor plane, to obtain maximum resolution on the side where the blades move downward [for the standard array position (i.e., upwind of the turbine)] and where maximum noise radiation was observed in the 2005 campaign. The array had a high microphone density in the center to ensure low side-lobe levels at high frequencies and had a low-density outer part to obtain a good resolution at low frequencies [37]. The distance and orientation of the array with respect to the turbine were determined using a laser distance meter and a compass.

B. Data Acquisition

Acoustic data from the array microphones were synchronously measured using the VIPER multichannel data-acquisition system [38] at a sample frequency of 30.7 kHz and a measurement time of 30 s. The acoustic data were processed using fast Fourier transform blocks of 1024 samples with a Hanning window and 50% overlap, yielding 1800 averages and a narrowband frequency resolution of 30 Hz. A second-order 500 Hz high-pass filter (-12 dB/octave [38]) was used to suppress high-amplitude pressure fluctuations at low frequencies and thus to extend the dynamic range of the A/D converter, so that low-pressure amplitudes at high frequencies were

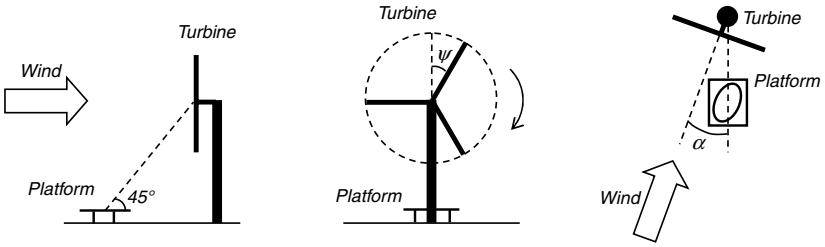

Fig. 3 Side view (left), front view (middle), and top view (right) of the test setup. The array microphones were mounted on the platform in an elliptic shape for optimum resolution.

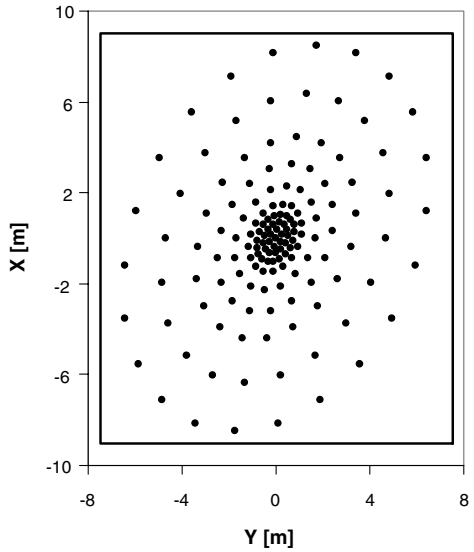

Fig. 4 Layout of array microphones. The rectangle indicates the platform dimensions.

included. The sound levels were corrected for the filter response and for pressure doubling due to reflections at the platform. Before the measurements, the sensitivity at 1 kHz was determined for all array microphones using a calibrated pistonphone. The frequency response of the Panasonic microphones was taken from previous calibration measurements. The frequency response of the M51 microphones was taken from calibration sheets. No corrections were applied for microphone directivity, because calibration measurements showed that these effects amounted to less than 2 dB up to 20 kHz for angles smaller than 75 deg with respect to the microphone axis. Phase matching of the microphones was checked using a calibration source at known positions. A trigger signal from the turbine (one pulse per revolution) was recorded synchronously with the acoustic data to determine the location of the blades as a function of time for the source localization on the individual blades (Sec. II.D).

In parallel to the acoustic measurements, several parameters from the turbine and two nearby meteorological masts were continuously measured at a sample rate of 4 Hz or higher. These data included wind speed, wind direction, temperature, power production, turbine orientation (misalignment angle α), rpm, and blade pitch angle.

C. Test Program

During the 4-week test campaign, in total, more than 600 measurements were taken. Following the International Electrotechnical Commission norm for wind turbine noise measurements [39], it was attempted to obtain measurements at wind speeds (at 10 m height) between 6 and 10 m/s. The wind speed at 10 m height was calculated by multiplying the average wind speed measured at the nacelle by 0.70 (according to the standard wind profile from [39]). Because the array position was fixed and the wind direction varied, both up- and downwind measurements were performed. Measurements with a large misalignment angle α (see Fig. 3) were excluded from the analysis, because for very oblique view angles, the array resolution becomes poor. On the basis of the turbine operational data, the most stable measurements (i.e., small variation in wind speed, rpm, pitch angle, and turbine orientation) were selected for further analysis.

An overview of the selected measurements is given in Table 1. Because of unpredictable weather conditions, it was not possible to obtain measurements in each wind-speed bin, and for state 1, only downwind measurements were done. Because the clean rotor is considered to be most representative for the rotor during normal operation, and because the upwind measurements covered all relevant wind speeds, the focus of this paper will be on state 2a.

The average turbine and weather conditions for the different rotor states are listed in Table 2 (equal weights per wind-speed bin). As mentioned in Sec. II.A, the blade pitch angle (not to be confused with the twist distribution) is zero at low wind speeds and increases for higher wind speeds. To give an impression of the variation of the parameters within each state, this table also shows the standard deviation for each value defined as

$$\sigma = \sqrt{\frac{1}{N-1}\sum_{i=1}^{N}(x_i - \bar{x})^2}$$

Table 1 Number of selected measurements per wind-speed bin for each rotor state

	6 m/s	7 m/s	8 m/s	9 m/s	10 m/s
State 1 (tripped rotor; array downwind)	8	8	8	0	0
State 2a (clean rotor; array upwind)	7	8	8	8	6
State 2b (clean rotor; array downwind)	8	8	8	0	0

Table 2 Average weather and turbine parameters for each rotor state[a]

	$U10$, m/s	P, MW	rpm	α, deg	Blade pitch, deg
State 1	6.9	1.6 (0.1)	14.5 (0.2)	−204 (12)	0.0 (0.1)
State 2a	8.1	2.1 (0.1)	14.9 (0.0)	−2 (4.4)	5.1 (0.6)
State 2b	6.9	1.6 (0.1)	14.6 (0.1)	−183 (2.4)	0.0 (0.0)

[a]The standard deviation σ is indicated between parentheses.

with

$$\bar{x} = \frac{1}{N}\sum_{i=1}^{N} x_i$$

Note that the power, rpm, and blade pitch angle are not randomly distributed around the mean value, but depend on the wind speed according to the turbine control system. Therefore, the standard deviations for these parameters are based on linear curve fits through the measured data as a function of wind speed. Because the turbine had an automatic yaw system, the yaw angle (i.e., the difference between the wind direction and the turbine orientation) was assumed to be zero.

D. Phased-Array Processing

The microphone array data were processed using two different methods. With the first (stationary) method, noise sources in the complete rotor plane were localized using conventional beamforming [40]. Thus, noise from the rotor hub can be separated from blade noise, and it can be seen where in the rotor plane the blade noise is produced. The method shows the integrated effect of the three blades, averaged over the complete measurement time of 30 s (i.e., several revolutions).

The first step of this processing involves the calculation of an averaged cross-spectral matrix, which contains the cross powers of all microphone pairs in the array. To improve the resolution and to suppress background noise (e.g., wind-induced pressure fluctuations on the microphones), the main diagonal of the cross-power matrix (i.e., the auto powers) was discarded. A spatial window was applied to the microphone signals, which reduced the effective array size with increasing frequency and which corrected for the variation in microphone density over the surface of the array [37]. In this way, the array resolution at low frequencies was improved, and coherence-loss effects at high frequencies (due to propagation of the sound through the atmospheric boundary layer) were suppressed.

Acoustic source maps of the rotor plane were produced by electronically steering the array to a set of grid points and calculating the noise radiated from each of them. The scan grid, with a diameter of 140 m and a mesh width of 2 m, was placed in the rotor plane and rotated in accordance with the orientation of the turbine (depending on wind direction). The 4 deg tilt angle between the rotor axis and the horizontal plane was also taken into account. The effect of sound convection in the atmospheric boundary layer was taken into account by assuming a constant wind speed between the scan location and the microphones. This constant wind speed was calculated as the average wind speed between the rotor hub and the array center, as determined from the standard wind velocity profile in [39].

The narrowband acoustic source maps were summed to one-third-octave bands, and the source levels were normalized to a constant reference distance. The noise sources in the rotor plane were quantified using a source-power integration method [37]. This technique sums the source powers in (part of) the measured source map and corrects the results with a scaling factor obtained by performing a simulation for a monopole source at the center of the integration region. The thus-obtained integrated sound pressure level of the turbine, as measured at the array position, is similar to the apparent sound power level defined in [39]. All spectra presented in this paper are in one-third-octave bands. The accuracy of the integration method is discussed in the next section.

The second processing method employed three rotating scan planes to localize the (de-Dopplerized) noise sources on the three individual blades [rotating source identifier (ROSI)] [41]. This enabled a comparison of the noise from the different blades. The start position of the scan planes was determined using a trigger signal from the turbine that was recorded synchronously with the acoustic data. Acoustic source maps of the different blades were produced by electronically steering the array to a set of rotating grid points and calculating the noise radiated from each of them. The three scan grids were placed in the rotor plane at azimuthal positions corresponding to the three blades. The blade grids ran from 15 to 60 m in the radial direction, had a chordwise extent of 30 m, and had a mesh width of 1 m.

Similar to the first processing method, the narrowband acoustic source maps were summed to one-third-octave bands, and the source levels were normalized to a constant reference distance. The ROSI results show the noise sources on the individual blades, averaged over a specified part of the revolution. To distinguish between the noise production during the down- and upward movements of the blades, separate ROSI scans were done for blade azimuth angles ψ from 0 to 180 deg and from 180 to 360 deg (with 0 deg as the upper vertical blade position). To limit processing time, only the first rotor revolution after the start of each acoustic measurement was processed. The noise from the blades was quantified using a power integration method for moving sound sources [42], which is similar to the aforementioned integration method for the stationary rotor plane. The thus-obtained integrated sound levels represent the contribution of the different blades to the overall sound pressure level of the turbine, as measured at the array position.

E. Accuracy of Source Localization and Quantification

The relative position and orientation of the acoustic array and the wind turbine were determined using a laser distance meter and a compass. Nevertheless, there are a number of uncertainties in the localization method, which may cause a deviation between the measured and actual source positions. First, the blades are not located exactly in the rotor plane: the 4 deg rotor tilt angle is accounted for, but not the rotor cone angle and the bending of the blades outside the plane. Second, sound refraction by wind shear and sound convection by wind gusts are not accounted for; a constant wind speed is assumed. Third, the rotor rpm is assumed to be constant within one revolution. Therefore, the accuracy of the source localization technique was assessed by attaching a whistle to one of the blades for a short period of time, at a position unknown to the acoustic test team. After determining to which blade the whistle was mounted, the ROSI source maps were used to estimate the exact whistle position (Fig. 5). The thus-obtained source radius was found to deviate only 0.5 m from the actual radius, which is considered to be accurate enough for these tests. Figure 5 also illustrates that the scan resolution is sufficiently high to determine accurate, integrated, blade noise levels. From numerical simulations [43], it was found that as long as the distance between adjacent scan points is smaller than the main lobe width (i.e., the width at 3 dB below the peak level), the integrated levels are accurate.

The acoustic source maps were quantified using the power integration method described in the previous section. The accuracy of this method in terms of *absolute* sound pressure levels was verified by comparing the integrated rotor source maps with the measured sound pressure levels at the array microphones. If all the noise measured by the array microphones is due to the turbine rotor, these spectra should coincide. Figure 6 shows the spectra measured by the array microphones (array) and the reference microphone at the center of the array (refmic) versus the integrated spectra for the rotor (powint) and the three blades (ROSI). These spectra were averaged over all measurements in state 2a, were corrected for pressure

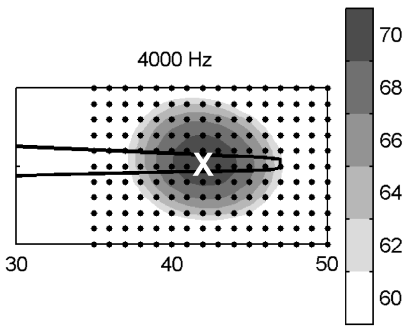

Fig. 5 Acoustic source map for whistle measurement. The black dots indicate the scan grid and the cross indicates the actual whistle position.

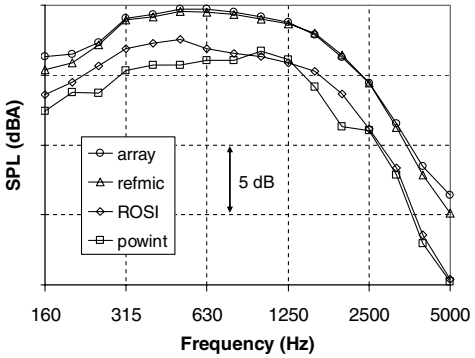

Fig. 6 Verification of power integrated method.

doubling by the array surface, and were normalized to the same reference distance. It can be seen that the average spectrum of the array microphones is practically equal to that on the reference microphone. The small difference at low and high frequencies may be due to wind noise on the array microphones at the edge of the platform.

Figure 6 also shows that the integrated spectra for the rotor and the blades have the same shape as the reference spectrum, but are about 3 dB lower over the whole frequency range. This discrepancy cannot be explained by the fact that the array method is applied to incoherent extended sources, because simulations for an incoherent line source yielded accurate integrated levels [37]. However, in addition to the aforementioned possible deviation between the rotor plane and the actual blade position, the observed difference may be partly explained by certain assumptions and simplifications in the integration method, such as the use of a single monopole source at the center of the integration region to determine the scaling factor for the source powers. For a simulated, realistic, wind-turbine-rotor noise source distribution, the difference between the actual and integrated overall rotor noise level was about 1 dB [25]. The difference may also be partly attributed to coherence loss at the array microphones, due to propagation of the sound through the turbulent atmospheric boundary layer. A similar effect has also been observed in open-jet wind-tunnel tests [37]. However, coherence-loss effects typically increase with frequency, whereas a more or less constant offset is found here. Furthermore, coherence-loss effects would be expected to increase with increasing wind speed, whereas the difference here between the integrated rotor noise level and the level of the reference microphone remained constant (within about 0.5 dB) for increasing wind speed. An alternative explanation for the lower integrated levels could be that the reference and array microphones pick up some background noise (e.g., from the wind over the platform), which is not present in the integrated rotor noise spectra (no background noise measurements with a stopped rotor were performed in the present test campaign).

The difference between the two integrated spectra may be due to the fact that the ROSI spectrum is de-Dopplerized and the rotor spectrum is not. For the down-going blade, de-Dopplerization results in reduced frequencies and reduced sound levels [due to convective amplification (see Sec. I)], and conversely for the up-going blade. Furthermore, the different integration regions (complete rotor versus outer part of the blades) will result in different scaling factors (depending on, for example, the side-lobe behavior [37]), which may lead to differences in the integrated spectra.

For the evaluation of the noise-reduction concepts in the present study, the accuracy of the *relative* sound levels (i.e., level differences between the different blades) was most important. This accuracy was assessed in the baseline test campaign by comparing the individual blade noise spectra for two consecutive revolutions: for each blade, the overall sound pressure level (averaged over all selected measurements) reproduced within 0.06 dB for the two consecutive revolutions, and the differences between the blades reproduced within 0.03 dB. It should be noted that due to the small difference in the out-of-plane blade loads (see Sec. I), the bending may be different for the three blades. Because the scan planes for all three blades are placed in the rotor plane, this may affect the measured noise differences between the blades. However, because the difference in bending between the blades can be estimated to be quite small (less than 0.25 m) on the basis of the load measurements and the spatial array resolution perpendicular to the rotor plane is limited, the systematical error in the noise difference can be determined to be less than about 0.05 dB (from array simulations). This means that the average level differences between the blades can be considered to be accurate within 0.1 dB for the given weather conditions, turbine operation parameters, and misalignment angle.

III. Results and Discussion

In this section, the results of the acoustic array measurements are presented and discussed. First, the noise source distribution in the rotor plane is analyzed for the up- and downwind array positions. Next, the noise sources on the individual blades are investigated, to assess the performance of the SIROCCO blade and the serrations as a function of array position, wind speed, and rotor azimuth angle. Because the clean rotor is considered to be most representative for the rotor during normal operation, and because the upwind measurements covered all relevant wind speeds, the focus will be on state 2a.

A. Noise Sources in the Rotor Plane

Each 30 s measurement resulted in acoustic source maps, showing the noise sources in the rotor plane as a function of frequency. To show the general trends, these maps were averaged over all selected measurements in the respective rotor state (Figs. 7–9). Thus, these maps show the average effect of all three blades over all revolutions. The black circle indicates the 94-m rotor diameter and the X indicates the center of the rotor plane. The range of the color scale is always 12 dB and the maximum is adjusted for each frequency band and each rotor state. The purpose of these source maps is to show the qualitative source characteristics; a quantitative comparison between the different rotor states will be made in Sec. III.B. The rotation direction is clockwise; note that the source maps in Figs. 7 and 9 are mirrored to allow easy comparison with the upwind measurements (i.e., an observer at the array position would see the rotor turn in the counterclockwise direction). Similar to the previous results on the baseline turbine [25], the upwind measurements (Fig. 8) indicate that for an observer at the array position, most of the noise is produced by

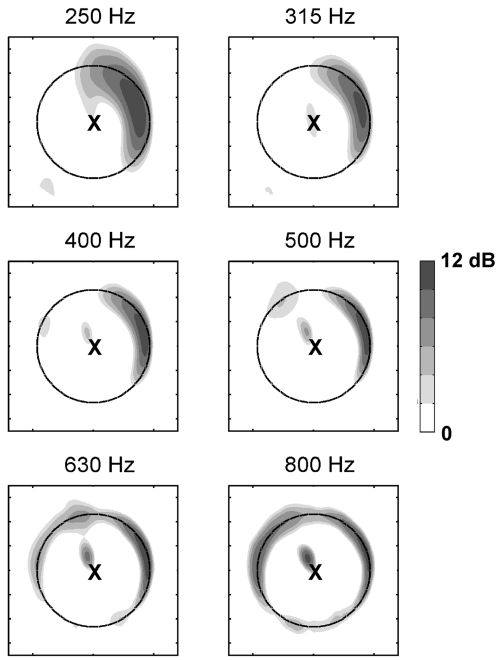

Fig. 7 Average stationary source maps for state 1 (tripped rotor, downwind array position). The range of the color scale is 12 dB and the maximum is adjusted for each frequency band.

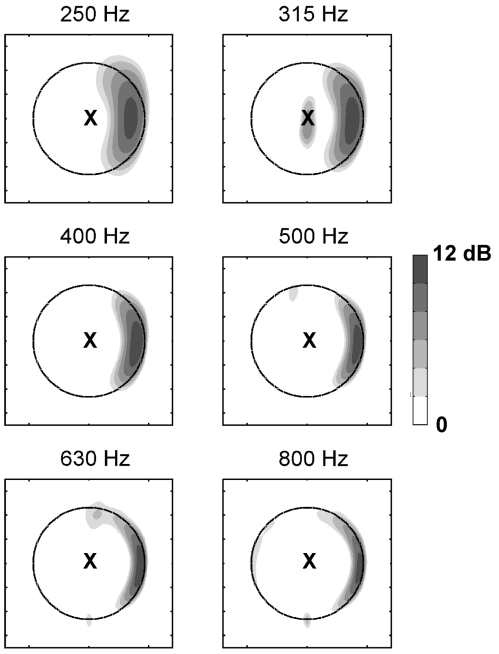

Fig. 8 Average stationary source maps for state 2a (clean rotor, upwind array position). The range of the color scale is 12 dB and the maximum is adjusted for each frequency band.

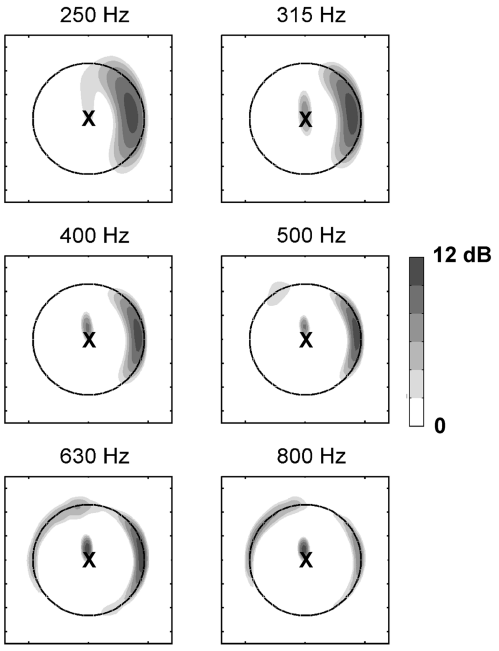

Fig. 9 Average stationary source maps for state 2b (clean rotor, downwind array position). The range of the color scale is 12 dB and the maximum is adjusted for each frequency band.

the outer 25% of the blades during their downward movement. This effect, which causes the typical swishing noise during the passage of the blades, can be explained by convective amplification and trailing-edge noise directivity [24], as described in Eq. (1). For the higher frequencies, minor noise sources can also be observed at the tip of the up-going blades and at the location where the blades pass the tower. The nature of this tower source is hard to assess on the basis of the present data, but it could originate from 1) reflection of blade noise on the tower, 2) impingement of blade tip vortices on the tower, and/or 3) the upstream influence of the tower on the flowfield around the blade.

For the *downwind* measurements (Figs. 7 and 9), nacelle noise appears to be more pronounced than for the upwind array position. In these plots, the nacelle source appears offcenter, because it is located in front of the scan plane, which coincides with the rotor plane. Only about 2.5 dB of the observed difference between the up- and downwind nacelle noise levels can be explained by the smaller distance to the array and the distance between the source and the scan plane. The remaining difference may be explained by a combination of two factors: First, mechanical noise generated inside the nacelle is radiated mainly in the downwind direction, because the ventilation opening is on the rear side of the nacelle. The relative nacelle noise level in state 1 is lower than in state 2b, probably because of the misalignment angle of −204 deg (i.e., a deviation of 24 deg with respect to −180 deg) in state 1 (see Table 2). Second, on the basis of the ξ dependence in Eq. (1), the trailing-edge noise from the blades is expected to be slightly higher on the upwind side than on the downwind side (due to the wind speed and rotor tilt angle). This was confirmed by comparison of the blade noise spectra in states 2a and 2b for the same wind-speed bins (see Sec. III.B.5). Despite the (relatively) increased nacelle noise, the overall turbine noise is still dominated by the noise from the blades.

Note that in Fig. 7, the source maximum for the down-going blade has shifted anticlockwise (relative to the state 2 plots), which can be explained by the convective amplification factor in Eq. (1) for the average misalignment angle of −204 deg in this rotor state [25]. Also note that in the downwind source maps the noise source at the tip of the up-going blades is more prominent than in the upwind maps. In the next section it will be shown that, in addition to a small directivity effect, this difference is mainly due to the lower average wind speed for these measurements (Table 2), which leads to a lower pitch angle and higher tip loading (see also Sec. II.A).

B. Noise Sources on the Individual Blades

As mentioned in Sec. I, acoustic field measurements on the baseline turbine [25] showed that the average OASPL for the two standard blades that were used again in the present campaign (i.e., the baseline and serrated blade) differed by less than 0.05 dB. Furthermore, it was argued in Sec. II.E that the average level differences between the blades, as measured with the microphone array, are accurate within 0.1 dB. Thus, with the present test setup it is well possible to assess the acoustic performance of the serrations and the new airfoil. In this section, the possibilities and limitations of acoustic measurements with a single microphone are first briefly discussed. Then the array results are used to study the average blade noise characteristics and the dependence on rotor azimuth, wind speed, observer position (upwind versus downwind), and rotor state (tripped versus clean blades).

1. Single-Microphone Analysis

In this section, the acoustic results of a single microphone are analyzed to demonstrate the possibilities and limitations of such measurements and to illustrate subjective onsite observations. During the field tests, the three different blades could be clearly distinguished by the difference in swishing noise produced during

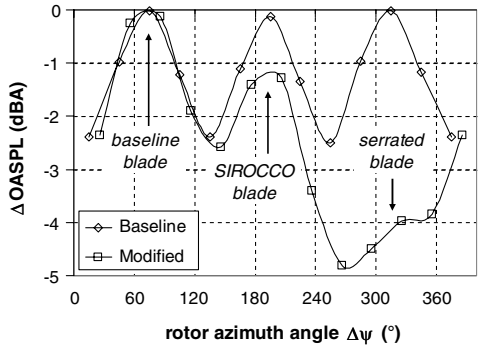

Fig. 10 Average sound pressure level on central array microphone as a function of rotor azimuth, for the baseline rotor (2005) and the rotor with modified blades (state 2a).

the passage of each blade. This can be illustrated by plotting the OASPL measured on a single microphone (i.e., the reference microphone at the center of the array) as a function of rotor azimuth angle (Fig. 10). The overall levels in this figure were summed between 250 and 800 Hz to focus on the low-frequency noise of the down-going blade. The result is *A*-weighted. Furthermore, the levels were averaged over all measurements and all revolutions in state 2a (synchronization was done using the trigger signal from the turbine). As a reference, the result for the test campaign on the baseline turbine (2005) is shown as well. Note that the results from the baseline rotor cannot be compared directly with those from the modified rotor, due to the different meteorological conditions. However, the *variation* in noise level between the three blades can be compared for the two test campaigns. For the baseline rotor, three humps are clearly observed, representing the swishing noise that is observed when the three blades pass the 3 o'clock position (see also Fig. 8). The three blades are practically equally noisy, and the amplitude variation (or swish) during the passage of the blades is about 2.5 dB. For the modified rotor, three humps with different amplitudes are observed, which can be associated with the baseline blade, the SIROCCO blade, and the serrated blade, respectively. Thus, it can be estimated that the SIROCCO blade yields a reduction of more than 1 dB, whereas the serrated blade is about 4 dB quieter than the baseline blade. However, it should be noted that these values only pertain to the low-frequency noise radiated from around the 3 o'clock position, whereas the blades may also produce significant noise during the other part of the revolution, as will be seen subsequently. Moreover, at each moment, the single microphone picks up the noise from all three blades, and so the contribution of each blade cannot be extracted from the single-microphone results. Thus, although Fig. 10 confirms subjective onsite observations, a dedicated array processing method (as described in Sec. II.D) is required to obtain a clear picture of the noise radiated by each individual blade during the complete revolution.

2. *Average Blade Noise Characteristics*

The source maps for the individual blades, averaged over one complete revolution and over all measurements in state 2a, are shown in Fig. 11. The source maps run from 15 to 60 m in radial direction and have a chordwise extent of 30 m. The black line indicates the outer 32 m of the blade (trailing edge on upper side). The range of the scale is 12 dB and the maximum is adjusted for each frequency band, so that the colors within one row can be compared directly. First, the source maps show that the differences in source *position* for the three blades are small. The source radial position, defined as the radius at which the maximum level in the source map occurs, is shown in Fig. 12 as a function of frequency for the three blades. Because the mesh size of the scan grid was 1 m (Sec. II.D), these source radial positions are multiples of 1 m. For all blades, the source radial position increases with frequency, which can be understood using the relation $St = f \cdot \delta^*/U \approx \text{const.}$ for the trailing-edge noise peak [6,33]; for increasing radius, the local blade inflow velocity U increases and the boundary-layer displacement thickness δ^* decreases, so that the produced frequencies are higher [24,25].

Except for the lowest frequencies, for which the modified blades have a lower source radius, the differences in average source radial positions between the different blades are small. More important, the source maps in Fig. 11 show that for low frequencies, both modified blades are significantly quieter than the baseline blade, especially the serrated blade. For high frequencies, however, both modified blades are noisier than the baseline blade, especially the SIROCCO blade. These trends are illustrated in Fig. 13, which shows the average integrated spectra for the three blades. These spectra were obtained by averaging the integrated spectra for all measurements in state 2a, with equal weights per wind-speed bin. As mentioned in Sec. II.D, these sound levels represent the contribution of the different blades to the overall sound pressure level of the turbine, as measured at the array position. The integrated spectra confirm the low-frequency noise reduction and high-frequency noise increase for the modified blades. For the serrated blade, the *A*-weighted sound pressure level at high frequencies is even higher than at low frequencies. The reasons

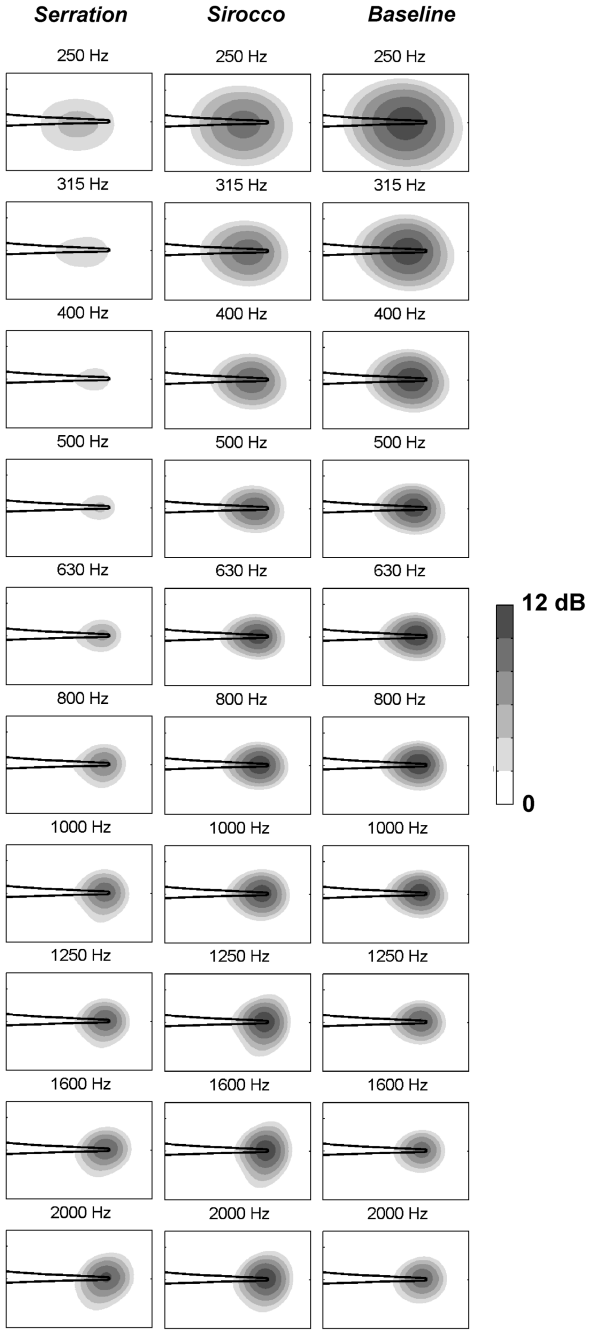

Fig. 11 Average rotating source maps for individual blades in state 2a, as a function of frequency. The range of the color scale is 12 dB and the maximum is the same within each row.

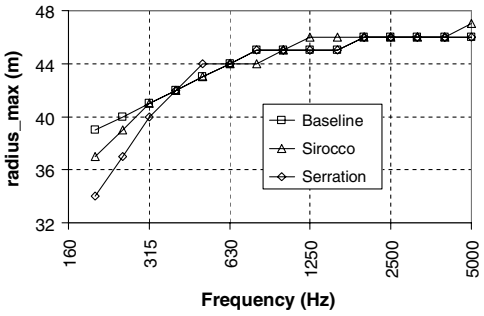

Fig. 12 Average source radial position as a function of frequency for the three blades in state 2a.

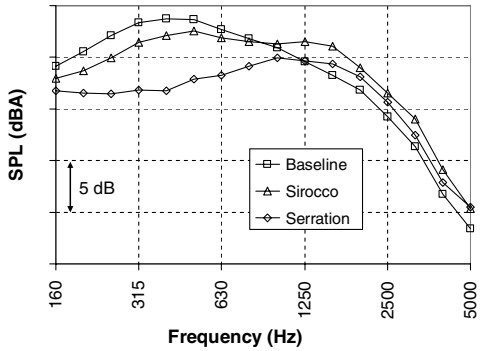

Fig. 13 Average blade noise spectra for state 2a.

for the increased noise level of the modified blades at high frequencies will be discussed in subsequent sections. Based on these average spectra, for the upwind measurements on the clean rotor (i.e., state 2a), which are considered most representative for normal operation and which cover all relevant wind speeds, average overall noise reductions of 0.5 and 3.2 dB were obtained for the SIROCCO and serrated blades, respectively. For the other two rotor states, which covered only the lower wind speeds, average noise reductions of 0.0 and 1.6 dB (state 1) and 0.2 and 1.2 dB (state 2b) were found for the SIROCCO and serrated blades, respectively. The reasons for the lower noise reduction in these states will be discussed in subsequent sections. The measurement uncertainty of the aforementioned average noise reductions will be discussed subsequently in Sec. III.B.4.

3. *Dependence of Blade Noise on Rotor Azimuth*

To better understand the acoustic behavior of the modified blades, it is interesting to look at the dependence of the blade noise on the rotor azimuth angle (Fig. 14). This figure shows the overall source maps for the different blades for 12 rotor azimuth intervals of 30 deg, starting at $\psi = 0$ deg (12 o'clock). These overall source maps (averaged over all measurements in state 2a) were obtained by summing the source maps between 160 Hz and 5 kHz, after applying *A*-weighting and a correction for array resolution (which depends on frequency and blade position) to the levels. Thus, the OASPL of the blade is equal to the sum of all scan levels in a given source map. Similar to the previous blade source maps, the black line indicates the outer 32 m of the blade. The range of the color scale is 12 dB, and the maximum is the same for all maps, so that the colors can be compared directly. This figure shows that during the *downward* movement of the blades, both modified blades are substantially quieter than the baseline blade. However, during the *upward* movement, both modified blades are noisier. These observations are illustrated in Fig. 15, which shows the integrated blade spectra for the down- and upward halves of the revolution separately. The high-frequency noise increase for the modified blades occurs mainly during the upward part of the revolution, and for the serrated blade, the increased noise of the up-going blade even dominates the overall average spectrum.

4. *Dependence of Blade Noise on Wind Speed*

In addition to the rotor azimuth, the blade noise characteristics were also found to depend strongly on the wind speed. This is illustrated in Figs. 16 and 17, which show the integrated blade noise spectra for the 7 and 10 m/s bins of state 2a, respectively (the state 2b spectra in Fig. 16 will be discussed subsequently in Sec. III.B.5). The 7 m/s blade spectra show a high-frequency hump around 1250–1600 Hz, which is absent in the 10 m/s spectra. As seen in the previous section, this high-frequency noise is mainly produced during the upward movement and originates from the very tip of the blade (Figs. 11–14). Because the average blade pitch angle was 0 deg in the 7 m/s bin and higher in the 10 m/s bin, this suggests that the high-frequency noise at low wind speeds can be associated with the increased tip loading as a result of the lower pitch angle (see Sec. II.A for turbine operation details). This also explains the fact that the upgoing blades were noisier in states 1 and 2b than in state 2a (Figs. 7–9), because the average blade pitch angle was lower than in state 2a (Table 2). Apparently, this tip noise does not follow the trailing-edge noise directivity function described in Eq. (1), because it is mainly radiated during the upward movement of the blades. Figure 16 also shows that the tip noise is much more prominent for the modified blades than for the baseline blade, which is always dominated by trailing-edge noise. Thus, the adapted pressure distribution on the modified blades, possibly in combination with the slightly increased

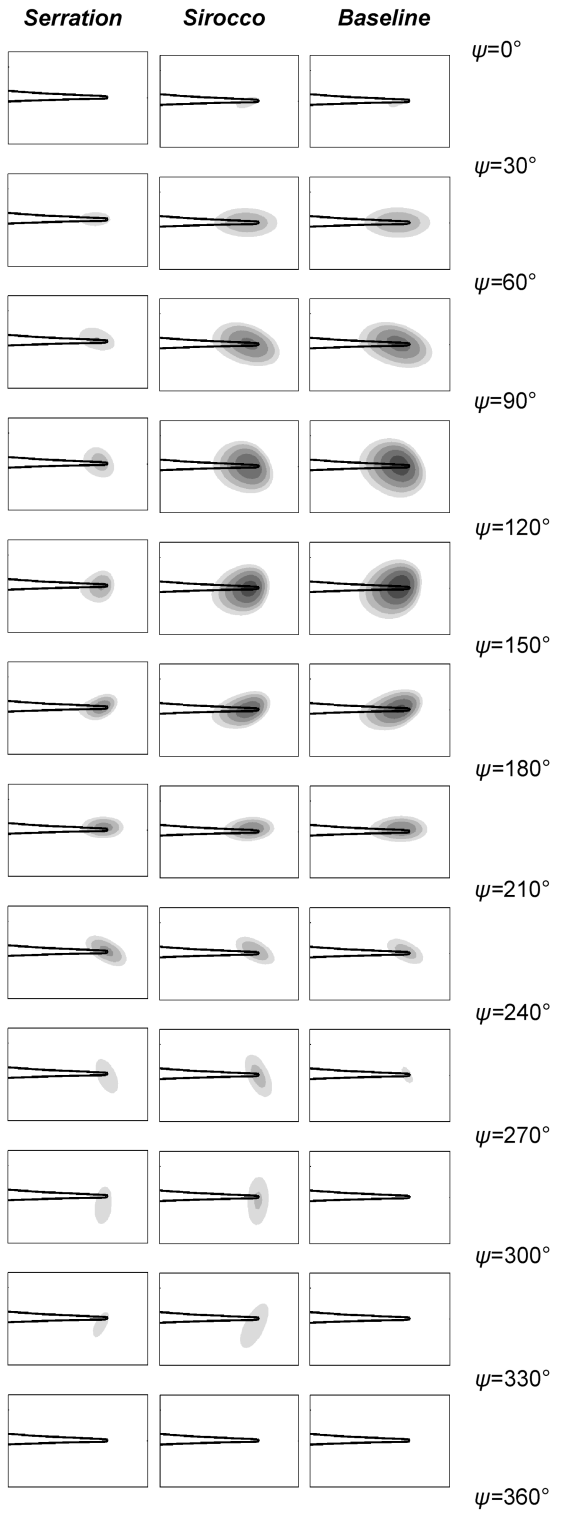

Fig. 14 Average overall source maps for individual blades in state 2a, as a function of rotor azimuth. The range of the color scale is 12 dB and the maximum is the same for all maps.

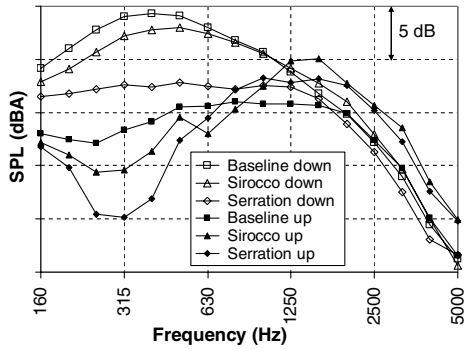

Fig. 15 Average blade noise spectra for the upward and downward part of the revolution in state 2a.

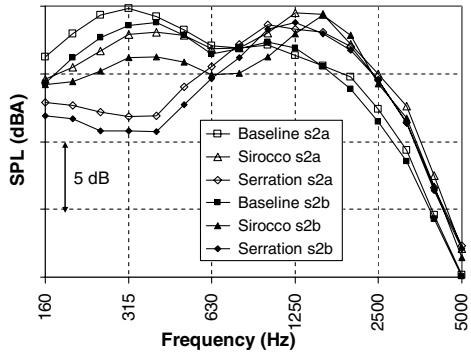

Fig. 16 Average blade noise spectra for the 7 m/s wind-speed bin of state 2a and state 2b.

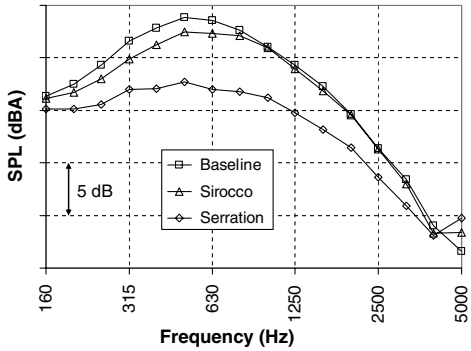

Fig. 17 Average blade noise spectra for the 10 m/s wind-speed bin of state 2a.

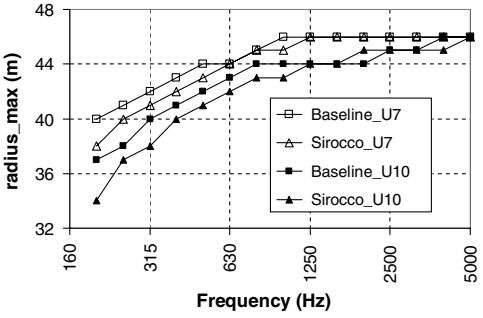

Fig. 18 Source radial position as a function of frequency for the baseline and SIROCCO blades in the 7 and 10 m/s wind-speed bins of state 2a.

blade loading (Sec. I), changes the tip vortex characteristics such that tip noise increases.

For the baseline and SIROCCO blades, the frequency of the low-frequency trailing-edge noise peak is higher at 10 m/s than at 7 m/s, which can be explained by the lower blade loading (due to the higher pitch angle), which leads to a thinner suction-side boundary layer. This is confirmed in Fig. 18, which shows the source radial positions for both blades in these two wind-speed bins: for a given radius, the trailing-edge boundary-layer thickness decreases for the higher wind speed, and so the produced frequencies are higher. For both bins, the source radial position of the SIROCCO blade is slightly lower than for the baseline blade, which is consistent with the higher trailing-edge noise-peak frequency and which suggests that the main objective of the airfoil design [i.e., to obtain a thinner suction-side boundary layer (see Sec. I)] has succeeded. If we suppress the spectral influence of tip noise by considering only the downward part of the revolution (Fig. 15), a slight trailing-edge noise increase is observed between 1 and 3 kHz for the SIROCCO blade, which, similar to the wind-tunnel results, can be attributed to the increased pressure-side boundary-layer thickness [35]. However, even if we consider only the downward part of the revolution, the average reduction in OASPL for the SIROCCO blade in state 2a is only 1.0 dB, which is lower than the 2–3 dB found in the wind-tunnel tests. The reasons for this discrepancy between wind-tunnel and field results are not fully clear yet. Apart from blade quality, a possible explanation could be that instationary inflow conditions in the field lead to lift fluctuations well beyond the prescribed design lift range [34].

In terms of *A*-weighted overall sound pressure levels (summed between 160 Hz and 5 kHz), both modified blades were found to reach maximum noise levels at a wind speed $U10$ of about 7 m/s, where the tip loading and therefore the tip noise are highest (the blade pitch angle only starts to increase significantly for wind speeds higher than 7 m/s). The noise from the baseline blade, which is dominated by trailing-edge noise, also peaks around 7 m/s. The corresponding noise *reductions* (Fig. 19) are lowest around 7 m/s and increase for higher wind speeds, for both the serrated and SIROCCO blades. Thus, the results indicate that at high wind speeds, the noise from the three blades is dominated by trailing-edge noise, which is effectively reduced by the new airfoil shape and the serrations. However, at lower wind speeds (increased tip loading due to lower pitch angle), significant high-frequency tip noise is generated by both modified blades during their upward movement, which partly cancels the trailing-edge noise reduction. As a result, the average noise reductions obtained in states 1 and 2b, which had lower wind speeds and therefore lower average blade pitch angles (Table 2), were lower than the 3.2 and 0.5 dB found in state 2a for the serrated and SIROCCO blades, respectively.

To evaluate these average noise reductions, it is important to understand the uncertainty levels associated with the measurement method employed during this study. As argued in Sec. II.E, for the weather conditions and turbine operation parameters in state 2a, the measurement uncertainty of the average noise reductions is smaller

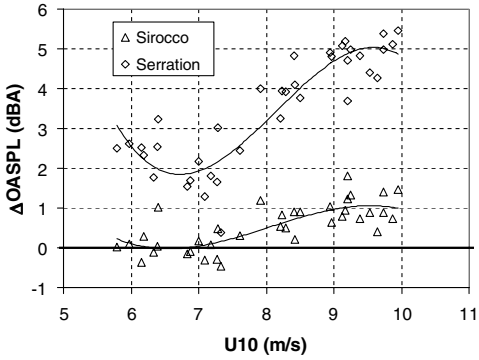

Fig. 19 Overall blade noise reduction as a function of wind speed for state 2a. The solid lines are third-order least-squares fits through the measured data.

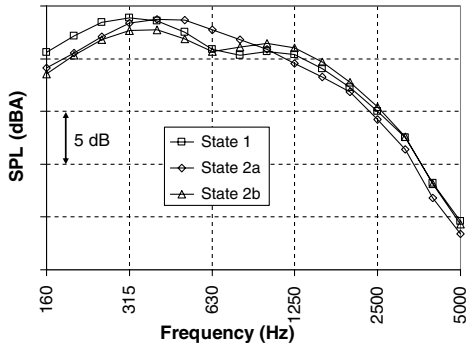

Fig. 20 Average baseline blade noise spectra for different rotor states.

than 0.1 dB. For different turbine and meteorological conditions (within the tested range), the uncertainty in the noise reduction can be assessed from the scatter in Fig. 19: for the serrated and SIROCCO blades, standard deviations σ of 0.6 and 0.4 dB were found, which leads to standard deviations of the mean ε for the *average* noise reductions of 0.10 and 0.06 dB, respectively. Because these ε values are smaller than the average noise reductions of 3.2 and 0.5 dB, the average reductions are significant for the tested range of turbine and meteorological conditions.

5. *Upwind Versus Downwind Measurements*

To assess the effect of observer location (i.e., upwind versus downwind array position), Fig. 16 compares the blade noise spectra for the 7 m/s bin in states 2a and 2b. The meteorological and turbine parameters were similar for both cases. It can be seen that the level of the low-frequency trailing-edge noise hump is lower on the downwind side for all three blades. A partial explanation for this could be that the downwind integrated blade noise levels suffer from increased coherence loss (see also Sec. II.E), because the blade noise propagates through the rotor wake. Indeed, the difference between the integrated rotor noise level and the level of the reference microphone was about 1 dB higher for the downwind measurements than for the upwind measurements in the 7 m/s bin. In addition, the reduced downwind trailing-edge noise levels may be explained by the ξ dependence in Eq. (1), due to the wind speed and rotor tilt angle (see also Sec. III.A). In contrast to the low-frequency noise, the high-frequency tip noise peak has approximately the same level for the up- and downwind measurements, which means that the *relative* importance of tip noise is higher on the downwind side. In addition to the tip loading effect discussed in the previous section, this increased importance of tip noise on the downwind side is an additional explanation for the lower noise reductions obtained in states 1 and 2b (as compared with state 2a) and for the fact that the up-going blades are noisier in states 1 and 2b than in state 2a (Figs. 7–9).

6. *Baseline Blade Noise for Different Rotor States*

Figure 20 shows the baseline blade noise spectra for the three different rotor states. With regard to the clean rotor, a number of differences can be observed between states 2a and 2b: First, the low-frequency trailing-edge noise peak for state 2a has a higher frequency and higher level than state 2b. This can be explained, respectively, by the higher wind speed (i.e., lower blade loading and thinner boundary layer) in state 2a and the difference in directivity for the up- and downwind observer positions (see Secs. III.B.4 and III.B.5). Second, state 2b spectrum shows a high-frequency tip noise peak, which is almost absent in state 2a. As mentioned before, this can be explained by the lower average wind speed (and thus higher tip loading) in state 2b (Sec. III.B.4) and by the increased importance of tip noise on the downwind side (Sec. III.B.5). Thus, to assess the influence of tripping on blade noise, state 1 should be compared with state 2b. The average conditions for these two states are practically the same, except for the misalignment angle (Table 2). Figure 20 shows that the low-frequency trailing-edge noise peak for state 1 has a higher level and lower frequency than in state 2b. This suggests that the trip has increased the trailing-edge boundary-layer thickness. Furthermore, the high-frequency tip noise peak is slightly lower for the tripped case. Thus, the results do indicate a small effect of tripping (0.6 dB increase in OASPL for the present conditions), but for a conclusive answer, measurements should be done with a clean blade and a tripped blade on one rotor.

IV. Conclusions

Acoustic field measurements were carried out on a 94-m-diam wind turbine, with one standard blade, one blade with an optimized airfoil shape, and one standard blade with trailing-edge serrations. The blade modifications had no adverse effect on their aerodynamic performance. To assess the effect of blade roughness due to dirt or insects, the blades were tested in both clean and tripped conditions. A large horizontal microphone array, positioned at a distance of about one rotor diameter from the turbine, was used to locate and quantify the noise sources in the rotor plane and on the individual blades. Because the array position was fixed and the wind direction varied, both up- and downwind measurements were performed.

The acoustic source maps for the baseline blade showed that for an observer at the array position, the dominant source was trailing-edge noise from the outer 25% of the blade. Because of convective amplification and directivity, practically all noise was produced during the downward movement of the blade, which caused the typical swishing noise during the passage of the blades. Both modified blades showed a significant trailing-edge noise reduction at low frequencies, which was more prominent for the serrated blade. However, the modified blades also showed a noise increase at high frequencies, which can be associated with the blade tips. This high-frequency tip noise was mainly radiated during the upward part of the revolution and was most important at low wind speeds (i.e., high tip loading) and for the downwind array position. Nevertheless, for the upwind measurements on the clean rotor, which were considered to be most representative for normal operation and covered all relevant wind speeds, average overall noise reductions of 0.5 and 3.2 dB were obtained for the optimized blade and the serrated blade, respectively. For both blades, the noise reduction increased with increasing wind speed. The downwind measurements on the clean and tripped rotors only covered the lower wind speeds and showed less noise reduction. Comparison of the noise from the baseline blade for clean and tripped conditions suggested a noise increase of 0.6 dB due to tripping.

Acknowledgments

Financial support for this research was given in part by the European Commission's Fifth Framework Programme, project reference SIROCCO (Silent Rotors by Acoustic Optimisation) (ENK5-CT-2002-00702). Financial support was also given by the Netherlands Organisation for Energy and the Environment (NOVEM). The authors would like to thank the colleagues from the University of Stuttgart and from the Netherlands Energy Research Foundation (ECN) for their valuable contributions to the definition of the tests and the interpretation of the results.

References

[1] Wagner, S., Bareiss, R., and Guidati, G., *Wind Turbine Noise*, Springer–Verlag, New York, 1996.

[2] Guidati, G., Ostertag, J., and Wagner, S., "Prediction and Reduction of Wind Turbine Noise: An Overview of Research Activities in Europe," AIAA Paper 2000-0042, 2000.

[3] Amiet, R., "Acoustic Radiation from an Airfoil in a Turbulent Stream," *Journal of Sound and Vibration*, Vol. 41, No. 4, 1975, pp. 407–420. doi:10.1016/S0022-460X(75)80105-2

[4] Howe, M. S., "A Review of the Theory of Trailing Edge Noise," *Journal of Sound and Vibration*, Vol. 61, No. 3, 1978, pp. 437–465. doi:10.1016/0022-460X(78)90391-7

[5] Blake, W. K., *Mechanics of Flow-Induced Sound and Vibration*, Academic Press, New York, 1986.

[6] Brooks, T. F., Pope, D. S., and Marcolini, M. A., "Airfoil Self-Noise and Prediction," NASA Ref. Publ. 1218, 1989.

[7] Dassen, T., Parchen, R., Guidati, G., Wagner, S., Kang, S., and Khodak, A. E., "Comparison of Measured and Predicted Airfoil Self-Noise with Application to Wind Turbine Noise Reduction," *Proceedings of the European Wind Energy Conference*, Irish Wind Energy Association, Slane, Ireland, Oct. 1997, pp. 422–428.
[8] Guidati, G., Bareiss, R., Wagner, S., Dassen, T., and Parchen, R., "Simulation and Measurement of Inflow-Turbulence Noise on Airfoils," AIAA Paper 97-1698, 1997.
[9] Hutcheson, F. V., and Brooks, T. F., "Effects of Angle of Attack and Velocity on Trailing Edge Noise," AIAA Paper 2004-1031, 2004.
[10] Oerlemans, S., and Migliore, P., "Aeroacoustic Wind Tunnel Tests of Wind Turbine Airfoils," AIAA Paper 2004-3042, 2004.
[11] Moreau, S., and Roger, M., "Competing Broadband Noise Mechanisms in Low Speed Axial Fans," AIAA Paper 2004-3039, 2004.
[12] Herr, M., and Dobrzynski, W., "Experimental Investigations in Low Noise Trailing Edge Design," AIAA Paper 2004-2804, 2004.
[13] Moriarty, P. J., Guidati, G., and Migliore, P., "Prediction of Turbulent Inflow and Trailing-Edge Noise for Wind Turbines," AIAA Paper 2005-2881, 2005.
[14] Grosveld, F. W., "Prediction of Broadband Noise from Large Horizontal Axis Wind Turbine Generators," AIAA Paper 84-2357, 1984.
[15] Glegg, S. A. L., Baxter, S. M., and Glendinning, A. G., "The Prediction of Broadband Noise from Wind Turbines," *Journal of Sound and Vibration*, Vol. 118, No. 2, 1987, pp. 217–239. doi:10.1016/0022-460X(87)90522-0
[16] Hubbard, H. H., and Shepherd, K. P., "Aeroacoustics of Large Wind Turbines," *Journal of the Acoustical Society of America*, Vol. 89, No. 6, 1991, pp. 2495–2508. doi:10.1121/1.401021
[17] Lowson, M. V., "Theory and Experiment for Wind Turbine Noise," AIAA Paper 94-0119, 1994.
[18] Fuglsang, P., and Madsen, H. A., "Implementation and Verification of an Aeroacoustic Noise Prediction Model for Wind Turbines," Risø National Lab., Risø-R-867(EN), Roskilde, Denmark, 1996.
[19] Lowson, M. V., Lowson, J. V., and Bullmore, A. J., "Wind Turbine Noise: Analysis of Results from a New Measurement Technique," AIAA Paper 98-0037, 1998.
[20] Moriarty, P., and Migliore, P., "Semi-Empirical Aeroacoustic Noise Prediction Code for Wind Turbines," National Renewable Energy Lab., Rept. TP-500-34478, Golden, CO, 2003.
[21] de Bruijn, A., Stam, W. J., and de Wolf, W. B., "Determination of the Acoustic Source Power Levels of Wind Turbines," *Proceedings of the European Wind Energy Conference*, H. S. Stephens and Associates, Bedford, England, U.K., Oct. 1984, pp. 889–894.
[22] van der Borg, N. J. C. M., and Vink, P. W., "Acoustic Noise Production of Wind Turbines in Practice," *Proceedings of the European Wind Energy Conference*, Hellenic Wind Energy Association and European Wind Energy Association, Oct. 1994, pp. 148–155.
[23] Hagg, F., van Kuik, G. A. M., Parchen, R., and van der Borg, N. J. C. M., "Noise Reduction on a 1 MW Size Wind Turbine with a serrated Trailing Edge," *Proceedings of the European Wind Energy Conference*, Irish Wind Energy Association, Slane, Ireland, Oct. 1997, pp. 165–168.
[24] Oerlemans, S., Sijtsma, P., and Méndez López, B., "Location and Quantification of Noise Sources on a Wind Turbine," *Journal of Sound and Vibration*, Vol. 299, Nos. 4–5, 2007, pp. 869–883. doi:10.1016/j.jsv.2006.07.032
[25] Oerlemans, S., and Schepers, J. G., "Prediction of Wind Turbine Noise and Comparison with Experiment," *Proceedings of the Second International Meeting on Wind Turbine Noise* [CD-ROM], Inst. of Noise Control Engineering, Merseyside, England, U.K., Sept. 2007.
[26] Brooks, T. F., and Burley, C. L., "Rotor Broadband Noise Prediction with Comparison with Model Data," AIAA Paper 2001-2210, 2001.
[27] Schlinker, R. H., and Amiet, R. K., "Helicopter Rotor Trailing Edge Noise," NASA CR-3470, 1981.
[28] Dowling, A. P., and Ffowcs Williams, J. E., *Sound and Sources of Sound*, Ellis Horwood, London, 1983.
[29] Howe, M. S., "Noise Produced by a Sawtooth Trailing Edge," *Journal of the Acoustical Society of America*, Vol. 1, No. 1, 1991, pp. 482–487. doi:10.1121/1.401273
[30] Dassen, T., Parchen, R., Bruggeman, J., and Hagg, F., "Results of a Wind Tunnel Study on the Reduction of Airfoil Self-Noise by the Application of Serrated Blade Trailing Edges," *Proceedings of the European Wind Energy Conference*, H. S. Stephens and Associates, Bedford, England, U.K., 1996, pp. 800–803.
[31] Braun, K. A., van der Borg, N., Dassen, A., Doorenspleet, F., Gordner, A., Ocker, J., and Parchen, R., "Serrated Trailing Edge Noise (STENO)," *Proceedings of the European Wind Energy Conference*, James and James Science, London, Oct. 1999, pp. 180–183.
[32] Oerlemans, S., Schepers, J. G., Guidati, G., and Wagner, S., "Experimental Demonstration of Wind Turbine Noise Reduction Through Optimized Airfoil Shape and Trailing-Edge Serrations," *Proceedings of the European Wind Energy Conference*, WIP-Renewable Energies, Munich, July 2001, pp 351–354.
[33] Herr, M., "Design Criteria for Low-Noise Trailing Edges," AIAA Paper 2007-3470, 2007.
[34] Schepers, J. G., Curvers, A., Oerlemans, S., Braun, K., Lutz, T., Herrig, A., Wuerz, W., Matesanz, A., Garcillán, L., Fisher, M., Koegler, K., and Maeder, T., "Sirocco: Silent Rotors by Acoustic Optimisation," *Proceedings of the Second International Meeting on Wind Turbine Noise* [CD-ROM], Inst. of Noise Control Engineering, Merseyside, England, U.K., Sept. 2007.
[35] Lutz, T., Herrig, A., Würz, W., Kamruzzaman, M., and Krämer, E., "Design and Wind Tunnel Verification of Low Noise Airfoils for Wind Turbines," *AIAA Journal*, Vol. 45, No. 4, 2007, pp. 779–792. doi:10.2514/1.27658
[36] Herrig, A., Würz, W., Lutz, T., and Krämer, E.: "Trailing-Edge Noise Measurements Using a Hot-Wire Based Coherent Particle Velocity Method," Proceedings of the 24th AIAA Applied Aerodynamics Conference, San Francisco, AIAA Paper 2006-3876, June 2006.
[37] Oerlemans, S., Broersma, L., and Sijtsma, P., "Quantification of Airframe Noise Using Microphone Arrays in Open and Closed Wind Tunnels," *International Journal of Aeroacoustics*, Vol. 6, No. 4, 2007, pp. 309–333. doi:10.1260/147547207783359440
[38] Holthusen, H., and Smit, H., "A New Data-Acquisition System for Microphone Array Measurements in Wind Tunnels," AIAA Paper 2001-2169, 2001.
[39] *Wind Turbine Generator Systems—Acoustic Noise Measurement Techniques*, International Electrotechnical Commission Norm 61400-11, Geneva, 2002.
[40] Johnson, D. H., and Dudgeon, D. E., *Array Signal Processing*, Prentice–Hall, Upper Saddle River, NJ, 1993.
[41] Sijtsma, P., Oerlemans, S., and Holthusen, H., "Location of Rotating Sources by Phased Array Measurements," AIAA Paper 2001-2167, 2001.
[42] Sijtsma, P., and Stoker, R. W., "Determination of Absolute Contributions of Aircraft Noise Components Using Fly-Over Array Measurements," AIAA Paper 2004-2958, 2004.
[43] Broersma, L., "Acoustic Array Measurements—Airframe Noise and Wind Turbine Noise," M.S. Thesis, University of Twente, Enschede, The Netherlands, Jan. 2006.

J. Wei
Associate Editor